JOURNAL OF THERMOPHYSICS AND HEAT TRANSFER
Vol. 6, No. 2, April–June 1992

Laminar Impingement Jet Mach Number and Temperature Effects on Heat Transfer

Tarit Kumar Bose*
Indian Institute of Technology, Madras, India

A laminar, axisymmetric jet flow of an ideal gas impinging on an infinite flat plate has been studied for various jet exit Mach numbers, jet height to radius ratios, and jet exit temperature to wall temperature ratios by a time-dependent finite-difference method applying the Lax-Wendroff single-step scheme. From the field calculations of temperature and flow, the friction coefficient and Stanton number at the wall are evaluated. Stagnation wall pressures are compared with those behind a normal shock for a supersonic jet and with an isentropic compression for a subsonic jet. All of the flow parameters, the friction coefficient, and the heat transfer are dependent on the jet exit Mach number, the jet height to radius ratio, the jet exit to wall temperature ratio, the Prandtl number, and the jet exit Reynolds number.

Nomenclature

c = sonic speed, m/s
c_f = friction coefficient
c_p = specific heat at constant pressure, J/kg-K
D_j = jet diameter, m
E, F, G, H = vectors in Eqs. (3)
H = jet height, m
H^* = nondimensional jet height, H/R_j
h^0 = specific stagnation enthalpy, J/kg
K = a constant, Eq. (6)
K_T = a constant
k = heat conductivity coefficient, W/m-K
M = Mach number behind shock, Eq. (4b)
M_j = jet exit Mach number, u_j/c_j
M_s = stagnation-point Mach number at the edge of the boundary layer
M_∞ = freestream Mach number
Nu = Nusselt number, Eq. (5)
Pr = Prandtl number, $\mu c_p/k$
p = pressure, N/m^2
p_∞ = freestream pressure, N/m^2
p_j^0 = jet exit stagnation pressure, N/m^2
p_j = jet exit pressure, N/m^2
p_{w0} = wall pressure on axis
q_w = wall heat flux, W/m^2
R_b = outer boundary radius, m
R_j = jet radius, m, $D_j/2$
Re = Reynolds number, Eq. (5)
Re_j = jet Reynolds number, $\rho_j u_j D_j/\mu_j$
r = radial coordinate, m
r^* = nondimensional radial coordinate, r/R_j
St = Stanton number, Eqs. (5) and (7)
T = temperature, K
T_j = jet exit temperature, K
T_w = wall temperature, K
T_∞^0 = freestream stagnation temperature, K
T_∞ = freestream temperature
t = time, s
u_j = jet exit speed, m/s
v_r, v_z = velocity component in r, z directions, respectively
z = axial coordinate, m
z^* = nondimensional axial coordinate, z/R_j
z_{sonic} = height of the sonic point for supersonic jets
γ = specific heat ratio
μ = dynamic viscosity coefficient, kg/m-s
ρ = density, kg/m^3
ω = exponent for viscosity-temperature relation

Subscripts and Superscripts

j = jet condition
s = stagnation-point condition at edge of boundary layer
w = wall condition
0 = wall impingement point
* = nondimensional variable
∞ = freestream condition

I. Introduction

JET impingement heat-transfer study for various jet exit Mach numbers, jet height to diameter ratios, and jet exit temperature to wall temperature ratios has several important practical applications, for example, for plasmajets used for welding and cutting of metal plates, deposition of metals and ceramics on various material surfaces, estimation of cooling requirement for ground rocket launch pads, etc. A survey of available literature does not seem to indicate any study, even for a laminar case, on the effect of jet Mach number and jet exit Reynolds number.

In 1956, Glauert[1] studied the similarity solution of an impinging jet with small height in the boundary-layer region, which he called a wall jet. Smirnov et al.[2] experimentally studied heat transfer on a flat calorimeter between a submerged jet of water onto a plate held normal to the jet and gave expressions for Nusselt number against the corresponding jet diameter and Reynolds number. For small jet height, they conclude that the characteristic length is the height of the jet, but at larger jet heights, the characteristic length is the jet diameter to calculate the Reynolds number. Gardon and Akfirat[3,4] concluded from experiments that for nondimensional height H/R_j larger than 28, the lateral variation of the heat-transfer coefficient has a bell shape, whereas for the nondimensional height less than 16, humps begin to appear with well-defined secondary peaks on either side of the centerline. Miyazaki and Silbermann[5] gave friction coefficient and heat-transfer data for a two-dimensional, incompressible impinging jet, while dividing the entire impingement domain into four regions: 1) a stagnation region, where the freestream velocity increases quickly from zero to a maximum value; 2) a flat plate region with no pressure gradient; 3) a transition

Received Feb. 21, 1989; revision received Jan. 25, 1990; accepted for publication March 28, 1990.

*Professor, Department of Aerospace Engineering. Associate Fellow AIAA.

region in the boundary layer, where the velocity profile changes from a flat plate profile to that from the similarity solution; and 4) the similarity region. Sparrow and Lee[6] studied the heat transfer for a subsonic impinging jet by the method of solution by separation of variables. Martin[7] gave closed-form expressions for fluid velocity distribution and boundary-layer thickness for both two-dimensional and axisymmetric jets. Bouslog et al.[8] gave experimental results of the flowfield produced by rocket exhaust impingement and reported that the slope and location of the shock wave in between the rocket nozzle and the impinging wall depended on the jet height. Deshpande and Vaishnov[9,10] studied theoretically the flow in an impinging jet by using a relaxation procedure to solve incompressible flow equations written in terms of the stream and vorticity functions in an incompressible flow. The extent of the infinite flow was approximated by applying the boundary conditions at a finite but sufficiently large distance, whereas the tube exit velocity profile was assumed to be either a fully developed parabola or a flat profile. No heat transfer was calculated, but the results show a decrease in the peak friction coefficient for increasing Reynolds number at constant jet height or for increasing jet height for a constant Reynolds number (based on the jet diameter). Childs and Nixon[11] used a time-dependent method for solving a multiple impinging flow Mach number turbulent jet, but no heat-transfer calculations were made. Shayesteh et al.[12] did extensive measurements of turbulent jets that emerge from circular nozzles into a cross stream and then impinge on a flat surface perpendicular to the nozzle axis.

When an impinging jet issues into an environment that is at a temperature different from that of the jet, entrainment of the surrounding fluid affects the heat transfer to the wall. Striegel and Diller[13] defined an entrainment factor E.F. = $(T_j - T_{amb})/(T_j - T_w)$, where T_j, T_{amb}, and T_w are jet exit temperature, ambient temperature, and wall temperature, respectively. For $T_j = T_{amb}$ (E.F. = 0), the thermal entrainment[13] does not affect the heat transfer, but for $T_{amb} = T_w$ (E.F. = 1), there may be a significant effect on the heat transfer due to entrainment. While Striegel and Diller had computed heat flux for different values of the entrainment factor, it was conjectured by this author that for a jet temperature much greater than the ambient temperature, E.F. = 1 is a reasonable assumption. Whereas the assumption in the present analysis that the wall temperature is equal to the ambient temperature is a subset of the analysis of Striegel and Diller, the present completely numerical method is quite different from their method, in which different regions like the entrainment region, the impingement region, and the wall-jet region are treated separately. In the present paper, they are treated uniformly. Further, Striegel and Diller did not study the effect of the jet Reynolds number, which is one of the main purposes of the present paper.

From the above discussion of various references, it is evident that there has not been any effort to study the effects of the jet Mach number, jet Reynolds number, and the jet temperature to wall temperature ratio; the purpose of the present paper is to examine these variables. For a supersonic impinging jet, the pressure recovery at the stagnation point is shown to be dependent on the jet height and tends to approach the values for normal shock at infinite jet height. The sonic line is concave at smaller Mach numbers when viewed from the jet and is convex at higher Mach numbers, and the sonic line distance from the wall is dependent on the jet height, jet Mach number, and the jet to wall temperature ratio.

The present analysis is for a laminar axisymmetric jet of an ideal gas surrounded by the same ambient gas impinging on a flat plate to form a laminar boundary layer. It is assumed that the jet velocity and the thermodynamic state are uniform at the jet exit plane and are prescribed as input variables. The other input variables are the wall temperature, which is equal to the ambient temperature, the nondimensional jet exit height with respect to the jet radius, and the radial extent of the computational domain. Time-dependent flow equations are used in a fully conservative form with boundary-layer approximation for the laminar viscous terms. These are formulated in vector form, and the solution is obtained by the Lax-Wendroff single-step method. The method is in the class of time-dependent methods, which allow capturing of the shock ("shock capturing method") in a natural way, and a review of a number of numerical schemes has been given by Beam and Warming.[14] These methods, as a rule, do not allow sharp discontinuity of dependent variables (unlike in the "shock-fitting methods"), and in terms of keeping the length of the region of supersonic-subsonic transition small, some of the schemes such as the Lax-Wendroff or MacCormack[15] two-step schemes are only marginally superior to the single-step schemes such as that given by Lax-Wendroff. However, the disadvantages of using two-step schemes against the single-step schemes are that the former take double the computation time of the latter and cause "wiggles" in the distribution of the dependent variable near the foot of the shock. Taking everything into consideration, such as the speed and ease of calculation and the stability of the solution, the Lax-Wendroff single-step scheme was used for the present calculations. As a result, the normal shock for a supersonic impinging jet is replaced by the sonic line, and constant Mach number lines near the shock are somewhat distorted. Further, from the solution of the differential equations, friction and heat-flux results are evaluated in nondimensional form.

II. Analysis

The relevant fully conservative unsteady flow equations in boundary-layer approximation for an axisymmetric impinging jet (Fig. 1) written in vector form are

$$\frac{\partial}{\partial t}\begin{bmatrix} \rho r \\ \rho v_z r \\ \rho v_r r \\ (\rho h^0 - p) r \end{bmatrix} + \frac{\partial}{\partial z}\begin{bmatrix} \rho v_z r \\ (\rho v_z^2 + p) r \\ \left(\rho v_z v_r - \mu \dfrac{\partial v_r}{\partial z}\right) r \\ \left(\rho h^0 v_z - k \dfrac{\partial T}{\partial z}\right) r \end{bmatrix} + \frac{\partial}{\partial r}\begin{bmatrix} \rho v_r r \\ \left(\rho v_z v_r - \mu \dfrac{\partial v_z}{\partial r}\right) r \\ (p + \rho v_r^2) r \\ \left(\rho h^0 v_r - k \dfrac{\partial T}{\partial r}\right) r \end{bmatrix} - \begin{bmatrix} 0 \\ 0 \\ p \\ 0 \end{bmatrix} = 0 \tag{1a}$$

where

$$k \nabla T = (k/c_p)[\nabla h^0 - \tfrac{1}{2} \nabla (v_r^2 + v_z^2)] \tag{1b}$$

The boundary conditions for the solution of Eq. (1a) are $z = H$, $r < R_j$: M_j, T_j and p = ambient pressure are prescribed; $z = H$, $r > R_j$: $v_z = v_r = 0$ and p = ambient pressure; $z = 0$: $T = T_w$ = ambient temperature prescribed and gradient (p) normal to the wall is zero; $r = 0$: $\partial/\partial r = 0$, $v_r = 0$; and $r = R_b$: backward differencing of all variables.

Some explanations are needed to explain these boundary conditions. For steady ($\partial/\partial t = 0$) and no slip condition on the wall, the z-momentum equation, which is the second row in Eq. (1a), specifies automatically the condition that the gradient of pressure normal to the wall is zero. In addition, at $z = H$ and $r > R_j$, the condition $v_z = 0$ is replaced by $\partial v_z/\partial z = 0$ to consider the entrainment effect.

For $r \to 0$ (at the centerline), $v_r = 0$, and, after deleting the third row of Eq. (1a), the equation becomes

$$\frac{\partial}{\partial t}\begin{pmatrix}\rho\\ \rho v_z\\ \rho h^0 - p\end{pmatrix} + \frac{\partial}{\partial z}\begin{pmatrix}\rho v_z\\ \rho v_z^2 + p\\ \rho h^0 v_z - k\partial T/\partial z\end{pmatrix} + \begin{pmatrix}0\\ -\mu\partial^2 v_z/\partial r^2\\ -k\partial^2 T/\partial r^2\end{pmatrix} = 0 \tag{2}$$

In Eq. (2) the second derivative terms are obtained under the condition that at $r = 0$, $v_r = 0$ and $\partial/\partial r = 0$. Equation (1a) can now be written in the following vector equation form:

$$E_t + F_z + G_r + H = 0 \tag{3a}$$

In Eq. (3a) the subscripts t, z, and r denote partial derivative with respect to these coordinate variables, for which the single-step Lax-Wendroff scheme[14] is

$$E_{i,j}^{n+1} = [E_{i-1,j}^n + \Delta z_{i-1}(E_{i+1,j}^n - E_{i-1,j}^n)/(\Delta z_{i-1} + \Delta z_i)]/2 + [E_{i,j-1}^n + \Delta r_{j-1}(E_{i,j+1}^n - E_{i,j-1}^n)/(\Delta r_{j-1} + \Delta r_j)]/2 - (F_z + G_r + H)_{i,j} \cdot \Delta t \tag{3b}$$

where the superscripts n and $n+1$ are the respective time step indexes. Further, the partial derivative terms F_z and G_r are evaluated for unequal spatial grids.

The time step, because of the numerical stability,[15] is given by the so-called Courant-Friedrichs-Lewy (CFL) factor

$$\min[|v_r + c|\Delta t/\Delta r,\ |v_z + c|\Delta t/\Delta z] \leq \tfrac{1}{2}$$

where c is the local sonic speed, and Δr and Δz are minimum step size in the r and z directions, respectively.

While solving Eq. (1a) by the Lax-Wendroff single-step finite-difference scheme, we have a stable method to capture the shock, if any, in a natural way, but it does not capture the steep slope near the shock. Hence, the shock may be assumed to be located at a Mach number equal to unity (sonic line), and all flow properties near this line are continuous.

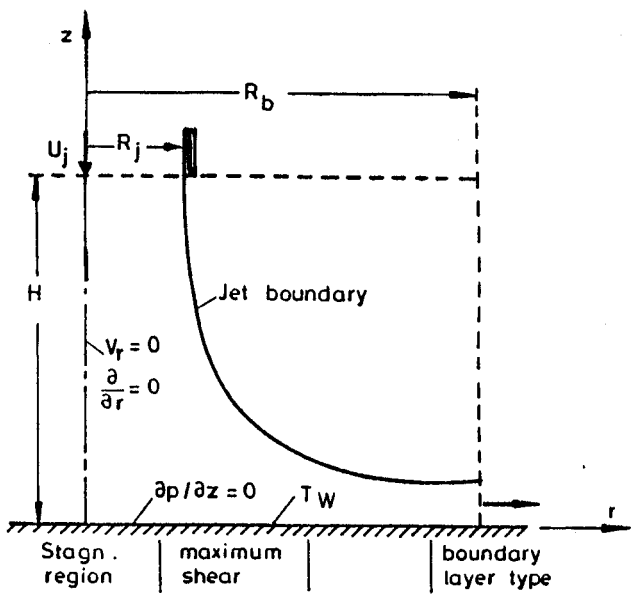

Fig. 1 Impinging jet model.

Table 1 Wall stagnation-point pressure to jet pressure ratio

M_j =	0.2	0.6	0.9	1.0	1.2	1.6	2.0
p_{w0}/p_j =	1.028	1.275	1.682	1.890	2.113	3.234	4.860

Table 2 Effect of Reynolds number Re_j on $c_{f,\max}$ and St_{j0}

M_j	T_j, K	H^*	D_j, m	Re_j	$c_{f,\max}$	St_{j0}
0.2	600	2	0.02	4.02,4[a]	1.101, − 4	3.85, − 5
0.2	600	2	0.01	2.01,4	2.202, − 4	7.70, − 5
0.2	600	20	0.02	4.02,4	1.696, − 5	1.38, − 5
0.2	600	20	0.01	2.01,4	4.062, − 5	2.62, − 5
2.0	600	2	0.02	4.02,5	1.078, − 5	8.10, − 6
2.0	600	2	0.01	2.01,5	2.156, − 5	1.62, − 5
2.0	600	20	0.02	4.02,5	9.979, − 5	2.28, − 6
2.0	600	20	0.01	2.01,5	1.996, − 6	4.56, − 4
0.2	900	2	0.02	2.58,4	1.342, − 5	3.56, − 5
0.2	900	2	0.01	1.29,4	2.684, − 4	7.12, − 5
0.2	900	20	0.02	2.58,4	1.576, − 5	1.01, − 5
0.2	900	20	0.01	1.29,4	3.153, − 5	2.01, − 5
2.0	900	2	0.02	2.58,5	1.317, − 5	6.10, − 6
2.0	900	2	0.01	1.29,5	2.635, − 5	1.22, − 5
2.0	900	20	0.02	2.58,5	9.405, − 7	1.37, − 6
2.0	900	20	0.01	1.29,5	1.881, − 6	2.74, − 6

[a] $4.02,4 = 4.02 \times 10^4$.

A. Wall Stagnation-Point Pressure

The results obtained from the field calculation are now compared with those from one-dimensional inviscid flow calculations. For subsonic inviscid flow, the ratio of the wall stagnation-point pressure to the jet exit pressure at $r = 0$ is given by the relation for isentropic compression

$$p_{w0}/p_j = [1 + (\gamma - 1)M_j^2/2]^{\gamma/(\gamma-1)} \tag{4a}$$

For supersonic inviscid flow, on the other hand, one has to take into account the loss in the stagnation pressure across the shock. If $\hat{(\ )}$ denotes the state behind a normal shock, the following relations from gasdynamics are used to determine p_{w0}/p_j:

$$\hat{M}^2 = \left[1 + \frac{(\gamma-1)}{(\gamma+1)}(M_j^2 - 1)\right] \Big/ \left[1 + \frac{2\gamma}{(\gamma+1)}(M_j^2 - 1)\right] \tag{4b}$$

$$p_j^0/p_j = [1 + (\gamma - 1)M_j^2/2]^{\gamma/(\gamma-1)} \tag{4c}$$

$$p_{w0}/p_j^0 = \left|\frac{2 + (\gamma-1)\hat{M}^2}{2 + (\gamma-1)M_j^2}\right|^{\gamma/(\gamma-1)} \left|\frac{(\gamma+1) + 2\gamma(M_j^2 - 1)}{\gamma + 1}\right| \tag{4d}$$

Equations (4a) and (4b–d) are used to calculate p_{w0}/p_j for subsonic and supersonic jet Mach numbers, respectively, the results of which are given in Table 1. It is expected, that, depending on the jet Mach number, the jet height, and the jet diameter (affecting the acceleration on the wall in the stagnation region), these values are the upper limit of the pressure ratio.

B. Comparison with Laminar Boundary-Layer Friction and Heat Transfer

The stagnation point on the wall for an impinging jet is somewhat analogous to the stagnation point of a sphere with the radius of curvature going to ∞. One can, therefore, attempt an analogous analysis.

For the blunt-body stagnation point for a flow around a spherically shaped nose of radius R_N, the friction coefficient is zero and the Stanton number relation is

$$St_s = \frac{q_w}{\rho_s u_s c_p (T_\infty^0 - T_w)} = \frac{Nu_s}{Pr \cdot Re_s}$$

$$= \frac{K}{Pr} \frac{\rho_w \mu_w}{\rho_s \mu_s} \frac{1}{Re_s^{0.5}} F(Pr, T_\infty/T_w, M_j) \tag{5}$$

where index s is the state at the edge of the boundary layer in the stagnation region (state behind the normal shock for a supersonic approaching flow), $Re_s = \rho_s u_s R_N/\mu_s$, and $Nu_s = q_w R_N/[k_s(T_\infty - T_w)]$. Further, the function F, which is the enthalpy gradient in the "local similarity coordinate," is dependent also on the "pressure gradient parameter" (= 0.5 for spherical nose). In addition, the constant K has the value $\sqrt{3} = 1.732$ for subsonic and low supersonic Mach numbers, but for high supersonic Mach numbers, one gets from modified Newtonian theory the expression

$$K = \frac{1}{M_s} \left| \frac{2}{\gamma} (1 - p_\infty/p_s) \right|^{0.5}$$

$$= \frac{1}{M_s} \left| \frac{2}{\gamma} \left\{ 1 - \frac{1}{1 + [2\gamma/(\gamma+1)](M_\infty^2 - 1)} \right\}^{0.5} \right|^{0.5} \tag{6}$$

It is estimated that for K, Eq. (6) is to be used if $M_\infty > 1.372$. Noting that in a normal shock $\rho_s u_s = \rho_\infty u_\infty$ and $St_\infty = St_s$ for the same heat flux for a boundary layer in the stagnation region of a sphere, the blunt-body stagnation heat transfer $Nu_s/Re_s^{0.5} = St_s \cdot Re_s \cdot Pr$ is independent of the Reynolds number Re_s. It will, however, be of interest to see whether this is true for the impinging heat transfer in the stagnation region also. Now for an impinging jet, the Stanton relation along the wall (including the stagnation region) is

$$St_j = \frac{q_w}{\rho_j u_j c_p (T_j^0 - T_w)} = \frac{k_w}{\rho_j u_j c_p (T_j^0 - T_w)} \left| \frac{\partial T}{\partial z} \right|_w \tag{7}$$

To study only the effect of the Reynolds number, jet Mach number M_j, jet exit temperature T_j, jet height $H^* = H/R_j$, and Prandtl number Pr are kept constant, and the jet diameter D_j is changed from 1 to 2 cm. Further, in all calculations, $T_w = 300$ K and $Pr = 0.7$ are assumed. Results of maximum friction coefficient $c_{f,\max}$ and the stagnation-point Stanton number St_{j0} are given in Table 2. It can be seen that both $c_{f,\max}$ and St_{j0} are inversely proportional to the jet Reynolds number. However, by allowing Re_j to go to ∞, these two quantities are likely to reach the limit of the infinite flow results, as discussed in standard textbooks on boundary-layer theory.

Similar to Eq. (7) for Stanton number, one can write for the impinging jet an expression for the friction coefficient as follows:

$$c_f = \frac{\mu_w}{\rho u_j^2} \left| \frac{\partial v_r}{\partial z} \right| \tag{8}$$

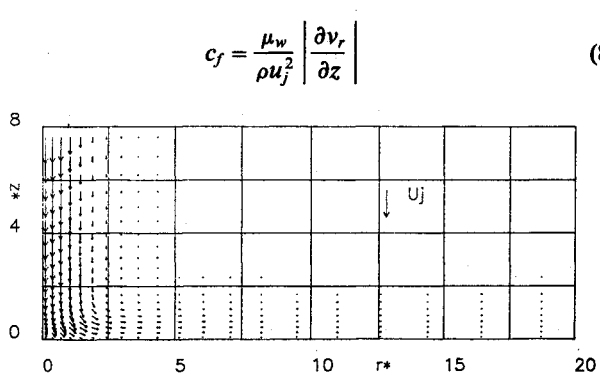

Fig. 2 Typical plot of velocity vectors for a subsonic impinging jet ($M_j = 0.2$, $T_j = 600$ K, $T_w = 290$ K, $Pr = 0.7$, $H^* = 8$, and entrainment allowed).

Table 3 Input values for some results for impinging jet

Serial no.	M_j	T_j, K	Pr	H^*	p_{w0}/p_j (field)	p_{w0}/p_j (Table 1)	z^*_{sonic} ($r = 0$)	$Nu_0/Re_j^{0.5}$
1	1.2	300	0.7	2	1.27	2.11	0.85	0.0727
2	1.6	300	0.7	2	1.35	3.23	0.58	0.0845
3	2.0	300	0.7	2	1.42	4.86	0.45	0.0956
4	0.6	600	0.7	2	1.14	1.27	—	0.0054
5	0.9	600	0.7	2	1.20	1.68	—	0.0050
6	1.2	600	0.7	2	1.26	2.11	0.83	0.0049
7	2.0	600	0.7	2	1.43	4.86	0.44	0.0058
8	0.6	900	0.7	2	1.13	1.27	—	0.0037
9	0.9	900	0.7	2	1.19	1.68	—	0.0033
10	1.2	900	0.7	2	1.26	2.11	0.83	0.0032
11	1.6	900	0.7	2	1.35	3.23	0.56	0.0031
12	2.0	900	0.7	2	1.43	4.86	0.45	0.0031
13	0.2	600	0.7	2	1.05	1.03	—	0.0076
14	0.2	600	0.7	4	1.08	1.03	—	0.0067
15	0.2	600	0.7	8	1.17	1.03	—	0.0041
16	0.2	600	0.7	15	1.20	1.03	—	0.0024
17	0.2	600	0.7	20	1.17	1.09	—	0.0024
18	2.0	900	0.7	2	1.43	4.86	0.45	0.0031
19	2.0	900	0.7	4	1.76	4.86	0.63	0.0026
20	2.0	900	0.7	8	2.82	4.86	1.64	0.0013
21	2.0	900	0.7	15	2.70	4.86	2.39	0.0007
22	2.0	900	0.7	20	2.60	4.86	3.04	0.0006
23	2.0	600	0.7	2	1.43	4.86	0.44	0.0058
24	2.0	600	0.7	4	1.78	4.86	0.56	0.0048
25	2.0	600	0.7	8	2.86	4.86	1.25	0.0026
26	2.0	600	0.7	15	2.77	4.86	2.31	0.0014
27	2.0	600	0.7	20	2.62	4.86	2.36	0.0014
28	0.2	600	0.5	2	1.05	1.03	—	0.0076
29	0.2	600	1.0	2	1.05	1.03	—	0.0076
30	0.2	600	1.5	2	1.05	1.03	—	0.0076
31	2.0	600	0.5	2	1.43	4.86	0.44	0.0051
32	2.0	600	1.0	2	1.43	4.86	0.44	0.0051
33	2.0	600	1.5	2	1.43	4.86	0.44	0.0051

In the similarity region of a laminar boundary layer over a flat plate, friction coefficient and heat-transfer expressions are well known and can be taken as

$$St_\infty \cdot Pr^{2/3} \cdot Re_\infty^{0.5} = 0.332 \quad \text{and} \quad c_f \cdot Re_\infty^{0.5} = 0.664$$

In the above expressions, $Nu_\infty = St_\infty \cdot Re_\infty \cdot Pr = q_w r/[k(T_\infty^0 - T_w)]$ and Re_∞ are based on the length coordinate along the plate r, and index ∞ refers to the state at the edge of the boundary layer. In addition, the above expressions have to be multiplied by[16]

$$K_T = [(1 + T_\infty/T_w)/2]^{(\omega - 3)/4}$$

where ω is an exponent in the relation for the dynamic viscosity coefficient $\mu \propto T^\omega$. For air, $\omega = 0.6$, and the viscosity relation used in the present calculations is $\mu = 1.87 \times 10^{-5} (T/300)^{0.6}$. In the above K_T there is a small correction due to M_∞ also, which may be neglected in the present case. Now, replacing T_∞ and other gas properties at the edge of the boundary layer formally by the jet temperature T_j and other corresponding properties at the jet exit, the following two expressions in the "local similarity" region of the boundary layer can be written:

$$Nu_\infty/Re_j^{0.5} = 0.47\, K_T/\sqrt{r^*} \quad \text{and} \quad c_f \cdot Re_j^{0.5} = 0.94\, K_T/\sqrt{r^*}$$

where $r^* = r/R_j$ and $Re_j = \rho_j u_j D_j/\mu_j$. For the purpose of comparison, we multiply the St_j value obtained from Eq. (7) by $Pr/\sqrt{Re_j}$ and the c_f value from Eq. (8) by $\sqrt{Re_j}$. These results are discussed in Sec. III.

III. Numerical Results and Discussion

The solution of Eq. (1a) is done for $T_w = 290$ K and for different input values of M_j, T_j, Pr, and $H^* = H/R_j$ (as given in Table 3), where R_T is the tube radius (Fig. 1) and subscript

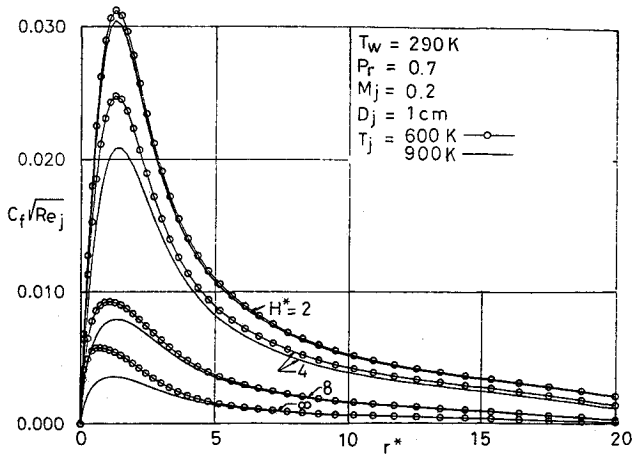

Fig. 3 Results of $c_f\sqrt{Re_j}$ vs r^* for different H^* and (T_j/T_w).

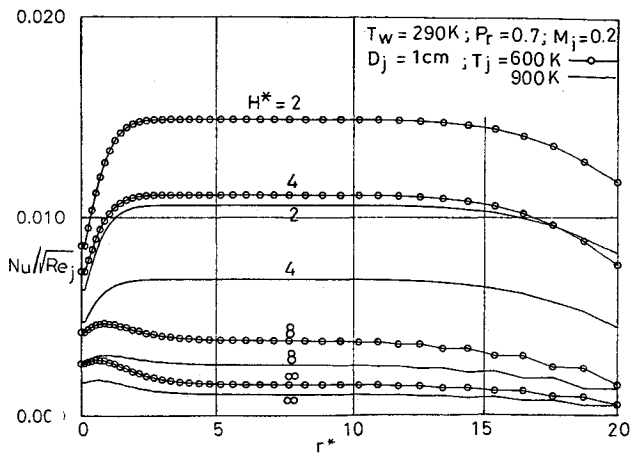

Fig. 4 Results of $Nu/\sqrt{Re_j}$ vs r^* for different H^* and (T_j/T_w).

j refers to the jet exit. In all calculations, p_j is equal to the ambient pressure of 1 bar, T_w to 290 K, and the maximum radial boundary to 20 times R_j. The total number of grid points are 41 in either the z or r directions, and the grids are in increasing step size in both directions. The step size is selected so that there are at least a reasonable number of grid points (around 8) near the wall and the axis at a distance of the order of the tube radius. Therefore, in the radial direction, a ratio of 1.06 for successive grid intervals was selected, and in the axial direction, this ratio was between 1.01 for $H^* = 2$ and 1.06 for $H^* = 20$. A CFL in the range between 0.15 and 0.4 based on the smallest grid size and the jet speed u_j is found to be adequate, but a lower value in the range is preferred for large H^*. Because these calculations have been carried out on a super-personal microcomputer, the total CPU time required was an important consideration. It was, therefore, felt that a convergence criterion for change better than 1% may be acceptable. Computation is carried out until $|\Delta v_z|/u_j$ and $|\Delta v_r|/u_j$ are less than a specified value (usually 0.007). Generally, about 50 time steps are enough to satisfy the above convergence criterion. At the jet exit plane, v_z, T_j, and p_j are assumed to be uniform. In addition, ambient temperature is equal to the wall temperature.

As a result of numerical calculation of the flowfield, local temperature, pressure, Mach number, and velocity components are computed, from which, further, the shear stress, heat flux, friction coefficient, Stanton number, and other variables along the wall are calculated. A sample velocity plot is shown in Fig. 2 for $H^* = 8$, $T_j = 600$ K, $M_j = 0.2$, and entrainment permitted. Table 3 also contains some of the results of the calculation. First, the wall pressure ratio at the stagnation point (p_{w0}/p_j), determined from field calculations, is given, followed in the next column by the values taken from Table 1. Generally, the (p_{w0}/p_j) results from field calculation are smaller than those taken from Table 1. For the supersonic jet Mach numbers it is quite evident, since the values in Table 1 are calculated under the assumption of a normal shock at the jet exit Mach number, but the actual shock position may be near the wall at lower Mach numbers. For subsonic Mach numbers around 0.2, the field calculation results are marginally higher than those in Table 1, which may be due to the constraint of using finite difference equations to solve the differential equations. From the preceding discussion, it is, therefore, evident that M_j and T_j/T_w are two important parameters for a given gas (Pr = const) and given jet diameter D_j. By keeping $T_w = 290$ K, $Pr = 0.7$, and $D_j = 1$ cm, $c_f\sqrt{Re_j}$ and $Nu/\sqrt{Re_j}$ are plotted in Figs. 3 and 4, respectively, for different values of H^* and T_j = 600 and 900 K, and in Figs. 5 and 6 for T_j = 900 K and $H^* = 2$ and and for different values of M_j, respectively. Analysis of these results shows a decrease in both friction coefficient and Nusselt number for increasing H^*, T_j, and M_j. Further, a summary of results is presented in Table 3, in which M_j, T_j (in K), Pr, and $H^* = H/R_T$ are input variables. In all calculations, wall temperature is kept equal to the ambient temperature (= 290 K). Similarly, the jet diameter D_j is equal to 1 cm in all cases mentioned in Table 3. The results presented in Table 3 by way of field calculation and by using Eqs. (4a–4d) are for the wall pressure on axis with respect to the jet pressure (= ambient pressure) ratio, p_{w0}/p_j, and the nondimensional sonic point height z^*_{sonic} and $Nu/\sqrt{Re_j}$

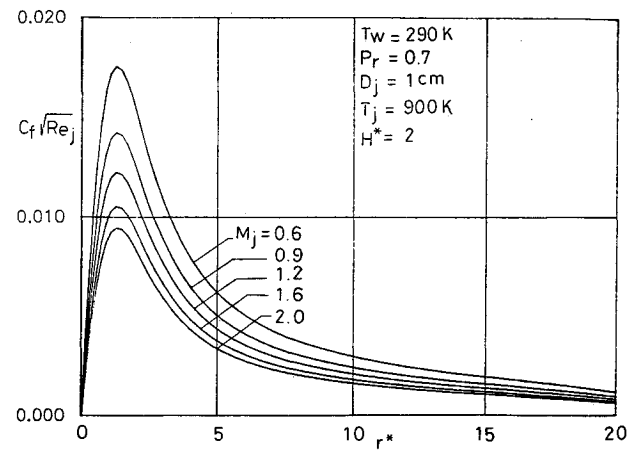

Fig. 5 Effect of M_j on $c_f\sqrt{Re_j}$ distribution for $H^* = 2$ and $T_j = 900$ K.

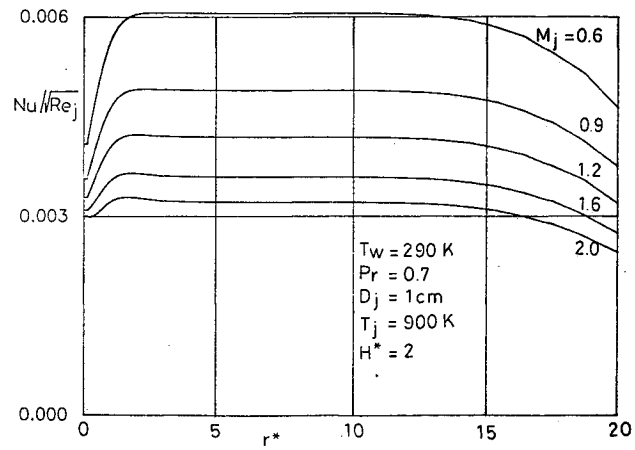

Fig. 6 Effect of M_j on $Nu/\sqrt{Re_j}$ distribution for $H^* = 2$ and $T_j = 900$ K.

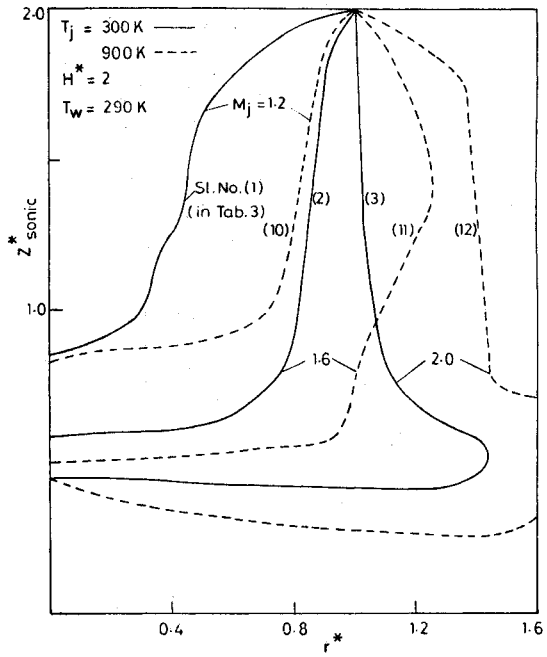

Fig. 7 Sonic lines for different M_j and temperature ratio for $H^* = 2$.

on the axis ($r^* = 0$). It can be seen from these results that for a subsonic jet, the pressure ratio (p_{w0}/p_j) is dependent on the jet height H^*. From the field calculation for $M_j = 0.2$, (p_{w0}/p_j) increases slightly as the jet height is increased from $H^* = 2$ to 20 with a maximum at around $H^* = 8$. These values from field calculations for the subsonic jet are generally slightly larger than those obtained from Eq. (4a), which is surprising and difficult to explain. For the supersonic jet, however, (p_{w0}/p_j) values determined from field calculations are always lower than those obtained from Eqs. (4b-4d) for a given H^*, and the difference between the two values increases with increasing M_j (increasing shock strength) for constant H^*, or with increasing H^* for constant M_j. It is evident that, for $M_j \geq 1$, the above height z^*_{sonic} decreases with increasing M_j, increasing temperature ratio T_j/T_w, and decreasing jet height H^*. Results for sonic line for $H^* = 2$ and different M_j and (T_j/T_w) are also given in Fig. 7. It is evident from Fig. 7 that while looking from the jet side, the sonic lines are concave for smaller Mach numbers, but they are slightly convex at higher Mach numbers. For a fixed M_j, the result is similar for decreasing jet height due to increasing acceleration near the wall, which results in increasing $c_{f,max}$ and higher $Nu_0/\sqrt{Re_j}$ on the axis ($r = 0$) at the wall. A comparison with flat plate results in the local similarity region of the impinged jet boundary layer is only qualitative, since, in the present case, the freestream $v_r \cdot r$ is approximately constant and not radial velocity constant, as in Ref. 5. As a result, decrease in the Nusselt number in the local similarity region is not as steep as in the two-dimensional case. For the $Nu_0/\sqrt{Re_j}$ value on the axis, again it was shown that this, for an impinging jet, is not independent of Re_j, and without knowledge of Re_j in Ref. 5, this could be compared only qualitatively.

IV. Summary and Conclusion

A completely numerical time-dependent method to study the laminar impingement friction and heat transfer in an axisymmetric jet solved by the Lax-Wendroff single-step scheme in variable grids has been presented. The results show the important effect of jet temperature, jet Mach number, and jet Reynolds number on the stagnation-point heat flux and maximum friction, in addition to the already known effect of the jet height. However, there are three important limitations in the present work. First, a somewhat ideal gas flow with constant specific heat and Prandtl number is considered. Second, turbulence and radiation effects are not considered, and third, the chosen Lax-Wendroff single-step scheme does not simulate the flow properties accurately in the shock region, which is, of course, the usual problem to a large extent in all numerical schemes. However, the present work is an important extension of results of references cited in this paper and can be extended further by removing the limitations in this paper.

Acknowledgments

This work was supported by the National Science Foundation under an International Cooperative Project Grant No. INT-8607177, and it was carried out in collaboration with C. J. Cremers, Department of Mechanical Engineering, University of Kentucky, Lexington, Kentucky.

References

[1]Glauert, M. B., "The Wall Jet," *Journal of Fluid Mechanics,* Vol. 1, 1956, pp. 625-643.

[2]Smirnov, V. A., Vervochkin, G. E., and Brdlick, M., "Heat Transfer Between a Jet and a Held Plate Normal to Flow," *International Journal of Heat and Mass Transfer,* Vol. 2, No. 1, 1961, pp. 1-7.

[3]Gardon, R., and Akfirat, J. C., "The Role of Turbulence in Determining the Heat Transfer Characteristics of Impinging Jets," *International Journal of Heat and Mass Transfer,* Vol. 8, No. 10, 1965, pp. 1261-1272.

[4]Gardon, R., and Akfirat, J. C., "Heat Transfer Characteristics of Impinging Two-Dimensional Air Jets," *Journal of Heat Transfer, Transactions of ASME (Series C),* Vol. 88, No. 1, 1966, pp. 101-108.

[5]Miyazaki, H., and Silbermann, E., "Flow and Heat Transfer on a Flat Plate Normal to a Two-Dimensional Laminar Jet Issuing from a Nozzle of Finite Height," *International Journal of Heat and Mass Transfer,* Vol. 15, No. 11, 1972, pp. 2097-2107.

[6]Sparrow, E. M., and Lee, L., "Analysis of Flow Field and Impingement Heat Transfer due to a Non-Uniform Slot Jet," *Journal of Heat Transfer, Transactions of ASME (Series C),* Vol. 97, No. 2, 1975, pp. 191-197.

[7]Martin, H., "Impinging Jet Flow Heat and Mass Transfer," *Advances in Heat Transfer,* edited by J. P. Hartnett and T. F. Irvine, Jr., Vol. 13, Academic Press, New York, 1977, pp. 1-60.

[8]Bouslog, S. A., Bertin, J. J., and Wingert, W. B., "Flowfield Produced by Rocket Exhaust Impingement on a Multitube Launcher," AIAA Paper 82-0946, 1982.

[9]Deshpande, M. D., and Vaishnov, R. N., "Submerged Laminar Jet Impingement on a Plane," *Journal of Fluid Mechanics,* Vol. 114, No. 1, 1982, pp. 213-236.

[10]Deshpande, M. D., and Vaishnov, R. N., "Wall Stress Distribution due to Jet Impingement," *Journal of Engineering Mechanics, Proceedings of the ASCE,* Vol. 109, No. 2, 1983, pp. 479-493.

[11]Childs, R. E., and Nixon, D., "Simulation of Impinging Turbulent Jets," AIAA Paper 85-0047, Jan. 1985.

[12]Shayesteh, M. V., Shabaka, I. M. M. A., and Bradshaw, P., "Turbulence Structure of a Three-Dimensional Impinging Jet in a Cross Stream," AIAA Paper 85-0044, Jan. 1985.

[13]Striegel, S. A., and Diller, T. S., "An Analysis of the Effect of Entrainment Temperature on Jet Impingement Heat Transfer," *Journal of Heat Transfer,* Vol. 106, No. 4, 1984, pp. 804-810.

[14]Beam, R. M., and Warming, R. F., "An Implicit Factored Scheme for the Compressible Navier-Stokes Equations. II: The Numerical ODE Connection," AIAA Paper 79-1406, 1979.

[15]MacCormack, R. W., "A Numerical Method for Solving the Equation of Compressible Viscous Flow," *AIAA Journal,* Vol. 20, No. 9, 1972, pp. 1275-1281.

[16]Bartz, D. R., "Heat Transfer from Rapidly Accelerating Flows," *Advances in Heat Transfer,* edited by J. P. Hartnett and T. F. Irvine, Jr., Vol. 2, Academic Press, New York, 1965.